crystals

MDPI

Article

Thermoelectrical Properties of ITO/Pt, In_2O_3/Pt and ITO/In_2O_3 Thermocouples Prepared with Magnetron Sputtering

Yantao Liu [1,*], Peng Shi [2], Wei Ren [2] and Rong Huang [1]

[1] Department of Electronic Engineering, Xi'an University of Technology, Xi'an 710048, China
[2] Electronic Materials Research Laboratory, Key Laboratory of the Ministry of Education & International Center for Dielectric Research, School of Electronic and Information Engineering, Xi'an Jiaotong University, Xi'an 710049, China
* Correspondence: liuyt@xaut.edu.cn

Abstract: ITO/Pt, In_2O_3/Pt and ITO/In_2O_3 thermocouples were prepared by the radio frequency (RF) magnetron sputtering method. The XRD results showed that all the annealed ITO and In_2O_3 films annealed at high temperature present a cubic structure. Scanning electron microscope results showed that the thickness of the ITO and In_2O_3 films could reach 1.25 μm and 1.21 μm, respectively. The ITO/Pt and In_2O_3/Pt thin film thermocouples could obtain an output voltage of 68.7 mV and 183.5 mV, respectively, under a 900 °C temperature difference, and at the same time, the Seebeck coefficient reached 76.1 μV/°C and 203.9 μV/°C, respectively. For the ITO/In_2O_3 thermocouple, the maximum value of the output voltage was 165.7 mV under a 1200 °C temperature difference, and the Seebeck coefficient was 138.1 μV/°C. Annealing under different atmosphere conditions under 1000 °C, including vacuum, air and nitrogen atmospheres, resulted in values of the Seebeck coefficient that were 138.2 μV/°C, 135.5 μV/°C and 115.7 μV/°C, respectively.

Keywords: ITO thin film; In_2O_3 thin film; thermocouples; magnetron sputtering

Citation: Liu, Y.; Shi, P.; Ren, W.; Huang, R. Thermoelectrical Properties of ITO/Pt, In_2O_3/Pt and ITO/In_2O_3 Thermocouples Prepared with Magnetron Sputtering. *Crystals* **2023**, *13*, 533. https://doi.org/10.3390/cryst13030533

Academic Editor: Hiroshi Yokoyama

Received: 24 February 2023
Revised: 13 March 2023
Accepted: 17 March 2023
Published: 20 March 2023

1. Introduction

With the continuous progress and development of the aviation industry, the performance of the engine, which is the core device of the aviation industry, is required to be more and more efficient, which requires the aero-engine to work stably in an extreme environment for a long time [1–3]. At the same time, the distribution of the temperature field inside the engine and the temperature value of high-temperature components are also necessary information in the process of engine design and improvement. Because it is easy to cause irreparable damage to the internal structural components of the engine under high-temperature conditions, it is necessary to control the internal temperature to avoid the erosion and other damage of the internal components caused by high temperature. [4] The high-temperature test of the aeroengine mainly includes the measurement of the internal combustion chamber wall, combustion chamber inlet and outlet gas, turbine blade surface, tail nozzle and other high-temperature components of the engine to obtain the temperature and distribution of these components. The data obtained from these tests are of great significance to the design and development of the engine [5]. Two kinds of measurement are performed for high-temperature components: contact and non-contact. The non-contact type uses the radiation signal issued by the measured components for measurement, such as infrared spectrum measurement [6,7] and the optical fiber method of measurement [8]. Contact measurement involves installing the temperature-sensing device on the surface of the component or integrated in the component, through the change of material characteristics or thermoelectric effect measurement. These methods include the crystal method [9–11], temperature paint method [12,13], and thermocouple method [14].

Thermoelectric tests can be conducted in two ways: standard armor and thin film thermocouple. The small thin film thermocouple can be easily integrated on the surface of

the high-temperature components and convert the thermal signal into an electrical signal, so that the real-time temperature value of the measured components can be obtained. In addition, the thickness of the thin film thermocouple is generally only in the order of micrometers, which can be ignored on the structure of the components. Further, it has the advantages of fast response, small thermal capacity and impact resistance [15,16], so it has therefore attracted considerable attention in the measurement of high-temperature components. There are many ways to prepare thin film thermocouples. Physical vapor deposition can be used on the surface of components, such as RF magnetron sputtering, DC sputtering, evaporation coating, etc. [17]. The application of thin film thermocouples to the testing of high-temperature engine components is suitable for the measurement of special extreme environments, such as the acquisition of the temperature parameters of engine turbine blades, combustion chamber walls and outlets, and provides accurate and reliable experimental data for design and improvement. Therefore, the design of thin film thermocouples and their application to high-temperature measurements have important practical significance.

With precious metal thin film thermocouples, such as Pt, Rh, WRe and other materials [18–20], the maximum measurable temperature is relatively low, and they are prone to failure conditions, such as falling off, oxidation, and large errors in extreme environments of high temperature, strong gas flow and strong corrosion. In addition, the Seebeck coefficient of precious metal thin film materials is small, resulting in small output voltage values. Therefore, it is necessary to select materials with better performance to replace noble metal materials as the electrodes of thin film thermocouples [21,22]. In order to solve many problems encountered by metals and their alloy materials in high-temperature engines, such as low resistance to high temperature, weak adhesion with the substrate, easy to fall off and easy to oxidize at high temperatures, oxide semiconductor materials have been selected because of the advantages of high-temperature resistance, corrosion resistance, oxidation resistance, etc. Moreover, their Seebeck coefficient is far greater than that of metal thin film materials, so they have also become an important direction for the selection of thin film thermocouple electrode materials [23–25]. With ITO/Pt thin film thermocouples on nickel-based substrates using alumina as insulating [26], the maximum test temperature can reach 1100 °C, the output value can reach about 50 mV, and the Seebeck coefficient can reach about 45 μV/°C.

In this study, ITO (In_2O_3, 10 wt% SnO_2), In_2O_3 and Pt films were successfully deposited on an alumina surface; the metal mask was used to form an electrode pattern; and the ITO/Pt, In_2O_3/Pt and ITO/In_2O_3 thermocouples were finally constructed. Laboratory tests were conducted to determine the properties of the thin film thermocouples. The microstructure of each of the ITO and In_2O_3 films was characterized in detail with an X-ray diffraction meter and scanning electron microscope. Moreover, the thermoelectrical performances of the ITO/Pt, In_2O_3/Pt and ITO/In_2O_3 thermocouples were systematically characterized.

2. Materials and Methods

ITO/Pt, In_2O_3/Pt and ITO/In_2O_3 thermocouples were deposited with the RF magnetron sputtering system (JPG-560, Sky Technology Development co., LTD., Shenyang, China). Figure 1 shows photographs of the ITO/Pt and In_2O_3/Pt samples. The ITO, In_2O_3 and Pt electrodes were 3 mm wide and 9.5 cm long, and the size of the substrates was 2 cm × 10 cm with a 1 mm thickness. The overlap area between the three kinds of electrodes on the hot junction area was about 3 mm × 3 mm. Al_2O_3 substrate with single-sided polishing was selected for the experiment, and ultrasonic cleaning was used to remove organic and inorganic substances on the surface of the silicon wafer. The cleaning process steps were as follows. The Al_2O_3 substrate was put into the culture dish, we added a proper amount of alcohol and acetone in turn, and each ultrasonic cleaning time was 10 min. After cleaning, the Al_2O_3 substrates were washed with deionized water, then dried with N_2, and were put into a drying oven at 100 °C for 30 min. After cleaning, the metal mask was placed on

the surface of the alumina substrate, and the ITO or In_2O_3 electrode pattern was formed on the surface of the substrate through the sputtering process. The diameter of the ITO and In_2O_3 target was 4 inches, and the sputtering parameters of the ITO and In_2O_3 films are as follows: the sputtering pressure was 2.0 Pa, the sputtering power was 100 W, the argon–oxygen ratio was 9:1, the sputtering time was 7 h. Then, all the ITO and In_2O_3 films were annealed at 1000 °C in a tubular furnace under an air atmosphere for 60 min. In order to characterize the effects of the annealing atmosphere on the performance of the thermocouple, three different atmosphere conditions of vacuum, air and nitrogen were used in the entire heat treatment of the prepared ITO/In_2O_3 thermocouple samples. A tubular furnace (OTF-1200, Kejing Materials Technology Co., LTD., Hefei, China) was used for heat treatment equipment. Under the condition of the vacuum atmosphere, the vacuum value was 6.0×10^{-1} Pa, and the heat treatment temperature was 1000 °C for 60 min.

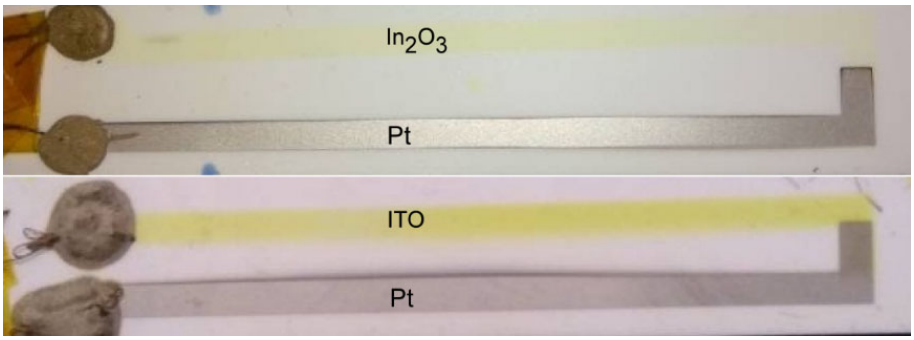

Figure 1. Physical images of ITO/Pt and In_2O_3/Pt samples.

After the ITO and In_2O_3 films were deposited on the Al_2O_3 substrate and annealed, another Pt electrode of the thermocouple was prepared by magnetron sputtering, and it formed a partial overlap area with the ITO or In_2O_3 electrode at the hot end. The Pt target with a diameter of 4 inches, thickness of 4 mm, sputtering pressure of 0.5 Pa, sputtering power of 100 W, and argon flow of 80 sccm was selected, and the sputtering time was 40 min. Before depositing the Pt film, the metal mask was placed on the surface of the alumina to form a Pt electrode. Enameled copper wire was used to connect the cold end of the thermocouple sample. The length of the copper wire was 20 cm, and the diameter was 0.5 mm. Silver paste was used as the adhesive, and the sample was dried at 150 °C for 30 min to ensure a good ohmic contact between the copper wire and the ITO and In_2O_3 films. The output voltage value of the system was measured and recorded by a data recorder (LR8431, HIOKI, Shangtian City, Japan), which can simultaneously record the voltage or temperature curve of 10 channels, and the voltage accuracy can reach 5 μV.

The structures of each ITO and In_2O_3 film sample were characterized with an X-ray diffraction meter (XRD, D/max-2400, Rigaku, Tokyo, Japan). The surface and cross-sectional SEM images were obtained with a field-emission scanning electron microscope (FESEM, Quanta 250 FEG, FEI, Portland, OR, USA). As Figure 2 illustrates, the test system consisted of the heating part, voltage acquisition, temperature acquisition at the hot and cold ends of the thermocouple, and a cooling unit. The heating unit was a high-temperature heating furnace (LHT 2-17, Nabertherm, Bremen, Germany). For the temperature measurement at the connection point of the hot end of the thermocouple, a WRP-100 standard S-armored thermocouple was used for testing the hot end of the thermocouple. The measurement range was in the range from room temperature to 1250 °C. Between the hot and cold ends, alumina foam transfer and high-temperature asbestos material were used for the insulation treatment, and the thermocouple sample was passed through the alumina foam brick to ensure a significant temperature difference between the two ends of the thermocouple, so as to obtain an accurate output voltage value. For the cold end of the thermocouple, the standard *K*-type thermocouple was used to measure the temperature of the cold junction.

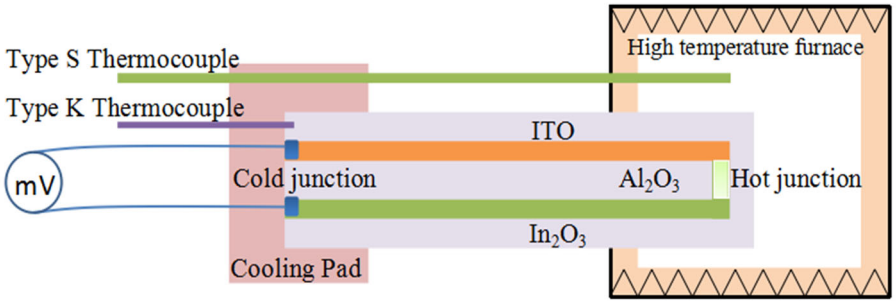

Figure 2. Schematic of ITO/In_2O_3 thermocouple test set-up.

Figure 3 illustrates the temperature change trends at the cold and hot ends of the thermocouples used in the experiment. During the heating process, the heating rate was set at 5 °C/min. During the entire heating process, the temperature at the cold end changed very little and remained at a lower temperature. Using the data recorder to obtain the temperature of the cold and hot ends at the same time, the temperature difference between the cold and hot ends of the thermocouple can be calculated. With the temperature difference as the abscissa, the thermal voltage of the thermocouple samples and the Seebeck coefficient as the ordinate, the change relationship curve of the output thermoelectric voltage, Seebeck coefficient and temperature difference of the thermocouple samples can be obtained.

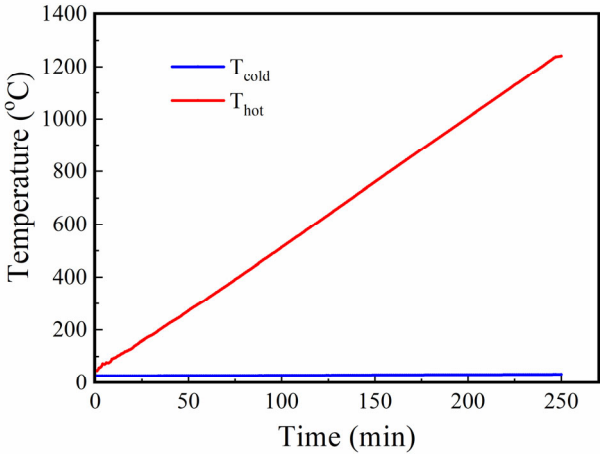

Figure 3. Temperature change curve of thermocouple cold and hot ends.

3. Results

3.1. Microstructure of ITO and In_2O_3 Thin Films

Figure 4 shows the XRD diffraction patterns of the ITO and In_2O_3 thin films after the heat treatment in the air atmosphere. It can be seen from the XRD diffraction results that the ITO and In_2O_3 films present a cubic structure, in which no characteristic diffraction peak of SnO_2 is observed, indicating that Sn atoms have entered the In_2O_3 structure to form a stable solid melt. After annealing, the (222), (400) and (440) peak strengths of the ITO and In_2O_3 films are obvious. Figure 5 shows the surface morphology and cross-section of the ITO and In_2O_3 films. After annealing at 1000 °C for 1 h, visible grains can be observed on the surface of the ITO and In_2O_3 films in Figure 5a,b. As there are no obvious cracks on the film surface, the rough film surface must have been caused by the high roughness of the alumina substrate. Figure 5c,d display the obvious fault structure of the ITO and In_2O_3 films, and the thickness of the ITO and In_2O_3 films could reach 1.25 μm and 1.21 μm, respectively.

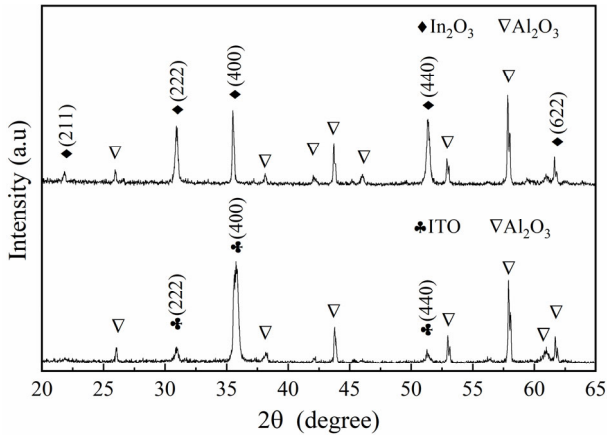

Figure 4. XRD patterns of ITO and In_2O_3 thin films.

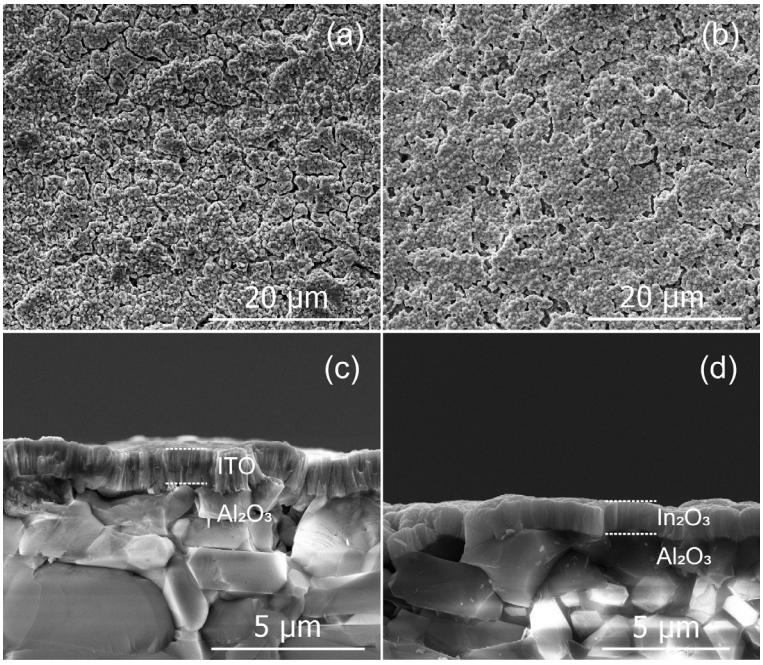

Figure 5. Surface morphology and cross-section of ITO film and In_2O_3 film: (**a**) ITO surface image; (**b**) In_2O_3 surface image; (**c**) ITO cross-section; (**d**) In_2O_3 cross-section.

3.2. Thermoelectrical Properties of ITO/Pt and In_2O_3/Pt

Figure 6a illustrates the relationship between the output thermal voltage of the ITO/Pt thin film thermocouple and the temperature difference between the cold and hot ends of the thermocouple. To prevent Pt electrode failure, the maximum temperature of the hot end was set at about 950 °C. As can be seen from Figure 6a, when the temperature difference between the cold and hot ends of the thermocouple reached 900 °C, the absolute value of its output voltage was 68.7 mV. Because ITO is an n-type semiconductor, its output was negative. Figure 6b shows that the Seebeck coefficient varied with the temperature. The Seebeck coefficient of the thermocouple increased linearly as the temperature difference increased. When the temperature difference between the cold and hot ends of the thermocouple reached 900 °C, the Seebeck coefficient was 76.1 μV/°C. It can be seen from the figure that the Seebeck coefficient of the ITO/Pt basically maintained a linear increasing trend in the low temperature section with the increase of the temperature. In the high-temperature section, especially when the temperature difference was close to 900 °C, the Seebeck coefficient showed a trend of slowing down. This phenomenon was caused by the interaction between the phonons and electrons in the material. According to the Kubakaddi

model, the Seebeck coefficient is composed of two parts: the sum of the components caused by electron diffusion and the components caused by phonon drag [27,28]:

$$S = S_d + S_g = \frac{2k}{e} - \frac{k}{e}\ln\left[\left(\frac{2\pi}{m^* kT}\right)^{\frac{1}{2}}\hbar n a^2\right] \quad (1)$$

where S is the Seebeck coefficient, n is the carrier concentration, k is the Boltzmann constant, $\hbar$ is the Planck's constant, e is the electron charge, a is the transverse dimension, and S_d is the Seebeck coefficient component due to diffusion, while S_g is the Seebeck coefficient component due to phonon drag.

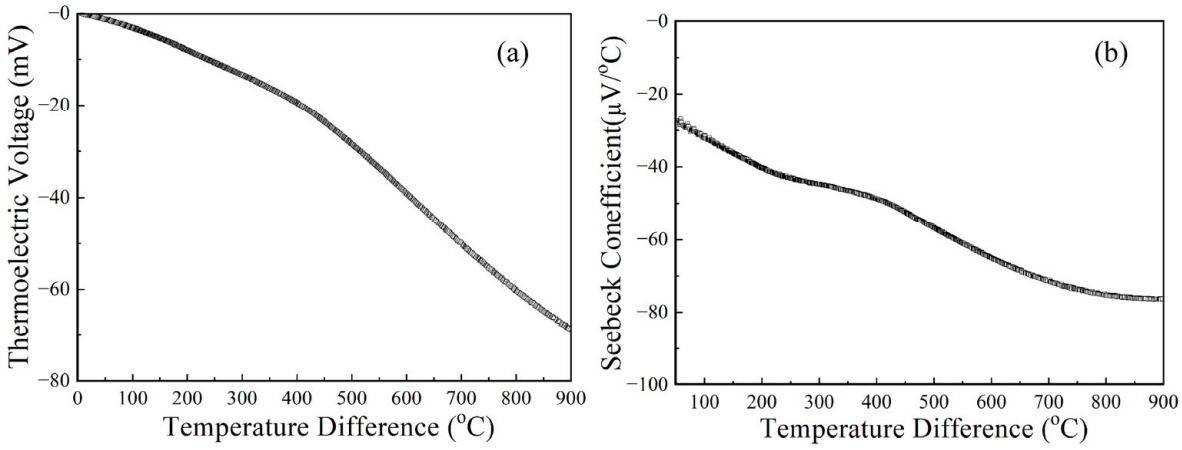

Figure 6. Thermoelectric response curve of ITO/Pt thermocouple. (**a**) Thermal voltage output; (**b**) Seebeck coefficient.

At the low-temperature stage, the electron diffusion component played a leading role, with a weak interaction between the phonons and electrons, so the Seebeck coefficient was relatively small. As the temperature rose, the interaction between the phonons and electrons became stronger. In the direction of the temperature gradient, along the direction of the thermocouple from the hot end to the cold end, the drag of the phonons on the electrons became more and more obvious, and the drag component of the phonons became stronger. Therefore, the Seebeck coefficient increased continuously and exhibited a linear-increase trend. With a further temperature increase at the hot end of the thermocouple, in the direction of the temperature gradient, the interaction among phonons played a leading role, and its drag on the electron became weaker. This inhibited the movement of the electron along the direction of the temperature gradient, slowing down the output of the ITO/Pt thin film thermocouple at high temperatures.

Figure 7a shows the relationship between the output thermal voltage of an In_2O_3/Pt thermocouple and the temperature difference between the hot and cold ends. When the temperature difference reached 900 °C, the absolute value of the output voltage was 183.5 mV. Figure 7b shows how the Seebeck coefficient varied with the temperature. The Seebeck coefficient of the thermocouple increased as the temperature difference increased. When the temperature difference between the hot and cold ends of the thermocouple reached 900 °C, the value of the Seebeck coefficient was 203.9 μV/°C. The Seebeck coefficient of the In_2O_3/Pt thermocouple also showed the same change trend. The drag effect of the phonons on electrons was greater at the cold end, and the rate of increase was faster, whereas at the hot end, the rate slowed down because of the interaction among the phonons.

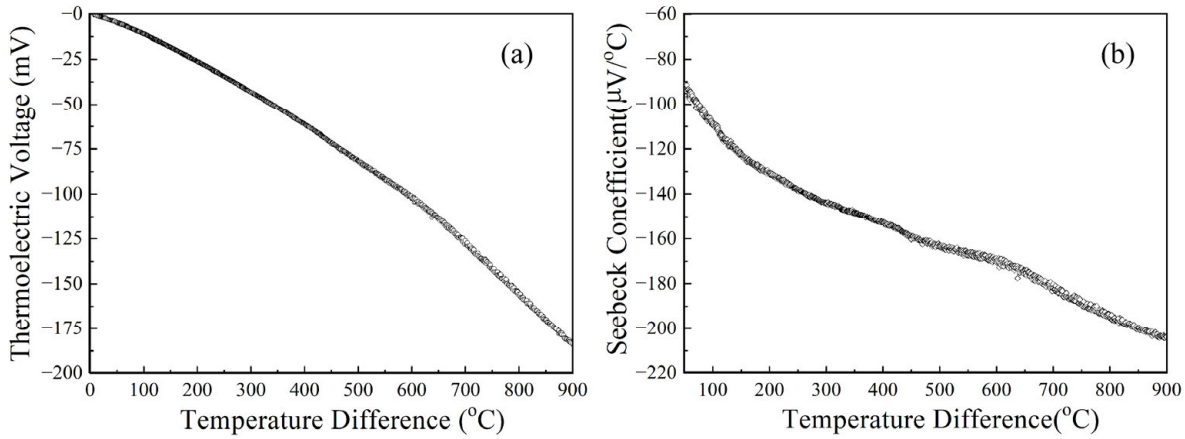

Figure 7. Thermoelectric response curve of In_2O_3/Pt thermocouple. (**a**) Thermal voltage output; (**b**) Seebeck coefficient.

For the output curves of the ITO/Pt and In_2O_3/Pt thermocouples, a cubic polynomials, namely, that expressed in Equation (2), was used to fit the results [29]:

$$E = A(\Delta T)^3 + B(\Delta T)^2 + C(\Delta T) + D \quad (2)$$

where E is the output thermal voltage of the ITO/Pt and In_2O_3/Pt thermocouples; ΔT is the value of the difference in the temperature between the cold and hot ends of the thermocouple; A, B, C and D are the coefficients of each part of the polynomial. The coefficient D is set to zero during fitting, because the output thermal voltage should be zero when the temperature difference between the cold and hot ends is zero, and the output thermal voltage output should be zero. The fitting results of the heating curve of the ITO/Pt and In_2O_3/Pt thermocouples are shown in Table 1, where the average Seebeck coefficient represents the average value of all the Seebeck coefficients of the thermocouples during all the heating stages and represents the fitting degree. As can be seen, the fitting degree of the two heating curves of the ITO/Pt and In_2O_3/Pt thermocouples was greater than 99.9%. According to the output thermal voltage value of ITO/Pt and In_2O_3/Pt, the output thermal voltage value of the ITO/In_2O_3 thermocouple can be deduced, and it should be the difference between the absolute values of the ITO/Pt and In_2O_3/Pt thermocouples. The average Seebeck coefficient of the ITO/In_2O_3 thermocouple can also be deduced, and it was approximately 127.8 μV/°C.

Table 1. Polynomial fitting results of ITO/Pt and In_2O_3/Pt thin film thermocouples.

Type	A (mV/°C^2)	B (mV/°C)	C (mV)	D	R^2	Seebeck Coefficient at 900 °C Difference (μV/°C)
ITO/Pt	3.592×10^{-8}	-1.001×10^{-6}	−0.017	0	0.9995	76.1
In_2O_3/Pt	-1.339×10^{-8}	-8.967×10^{-5}	−0.113	0	0.9998	203.9

3.3. Thermoelectrical Properties of ITO/In_2O_3

To characterize the output characteristics of the ITO/In_2O_3 thin film thermocouple, three calibration experiments were conducted calibrating the thermocouple with a thermocouple test system. As the results presented in Figure 8a illustrate, the output voltage of the ITO/In_2O_3 film thermocouple increased linearly with the increasing of the temperature. When the temperature difference between the cold and hot ends was 1200 °C, the temperature of the hot end was 1256 °C. The output of the thermocouple could reach 165.7 mV. The Seebeck coefficient of the thermocouple during three calibrations is shown in Figure 8b. When the temperature difference between the hot and cold ends was 1200 °C,

the maximum value of the Seebeck coefficient could reach 138.1 μV/°C. In addition, during the entire heating process, the Seebeck coefficient in the cubic calibration curve increased continuously with the rising of the temperature, and the rate of increase was faster in the low-temperature section, but slowed down in the high-temperature section. This was because the drag between the phonons and electrons in the low-temperature section was obvious, while the interaction among the phonons in the high-temperature section played a dominant role [30–32].

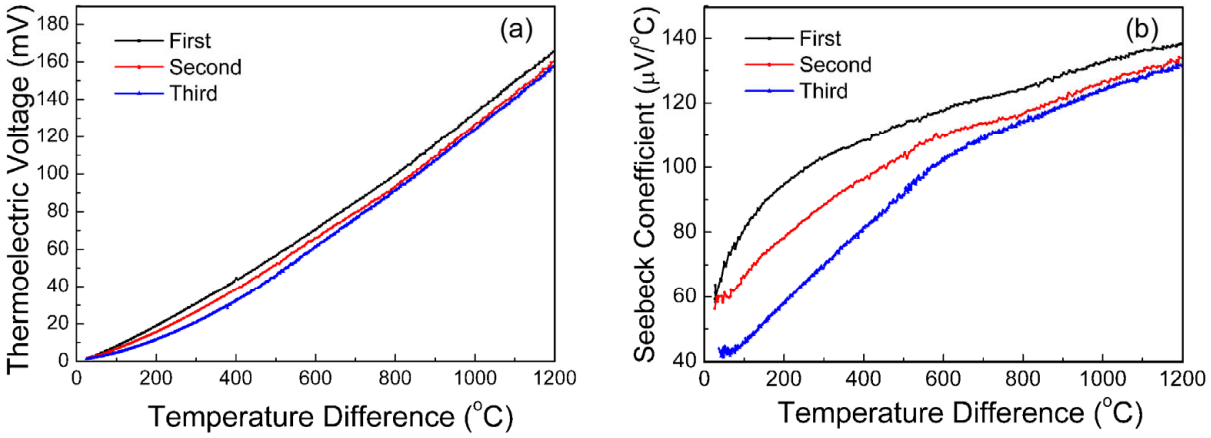

Figure 8. Output calibration and Seebeck coefficient change of In_2O_3/ITO thermocouple. (**a**) Thermal voltage output; (**b**) Seebeck coefficient.

In the calibration curve results of the third calibration experiment, the output value of the thermocouple also changed. This resulted from the hot end heating at a high temperature and the microstructure change of the film after heating. As can be seen, the calibration curves of the second and third experiments were closer, indicating that the performance of the thermocouple was stable. Table 2 shows the polynomial fitting results of the cubic calibration curves of the thermocouple. It can be seen that the values of all the calibrated curves were greater than 99.9%. In addition, the Seebeck coefficient of the entire heating process reached 138.1 μV/°C, which was higher than that of ITO/Pt (76.1 μV/°C) and lower than that of In_2O_3/Pt (203.9 μV/°C).

Table 2. Fitting results of output calibration polynomial of ITO/In_2O_3 thin film thermocouple.

Type	A (mV/°C^2)	B (mV/°C)	C (mV)	D	R^2	Seebeck Coefficient at 1200 °C Difference (μV/°C)
First	-1.609×10^{-8}	6.249×10^{-5}	0.084	0	0.9996	138.1
Second	-2.064×10^{-8}	7.959×10^{-5}	0.067	0	0.9992	134.2
Third	-4.824×10^{-8}	1.384×10^{-5}	0.034	0	0.9993	132.3

3.4. Effect of Annealing Atmosphere on Thermoelectric Properties

Figure 9a shows the thermoelectric output curves under different heat treatment atmospheres. The thermocouple samples prepared were heat treated under the three different conditions of vacuum, air and nitrogen. The heat treatment was conducted within a tubular furnace. For nitrogen heat treatment, the gas flow meter was adjusted to maintain the flow of N_2 at 50 sccm. The output voltage of the heat treatment under the N_2 atmosphere and vacuum conditions was lower than that of the heat treatment samples under the air condition during the entire heating process, especially under the N_2 atmosphere. The output curves showed good linearity under the three conditions. When the temperature difference between the hot and cold ends of the thermocouple was 1200 °C, the output of the thermocouple under the air, vacuum and N_2 atmospheres was 165.9 mV,

162.6 mV and 138.9 mV, respectively. The trend of the Seebeck coefficient variation trend of the thermocouple under the different heat treatment conditions is shown in Figure 9b. The Seebeck coefficient also increased in the duration of the heating process. When the temperature difference was 1200 °C, the Seebeck coefficients under the vacuum, air and N_2 atmospheres were 138.2 μV/°C, 135.5 μV/°C and 115.7 μV/°C, respectively.

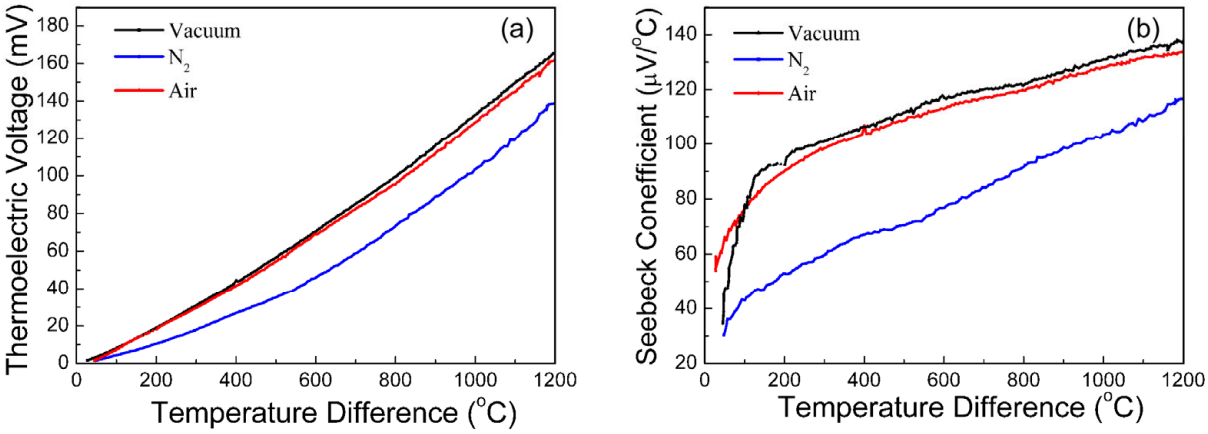

Figure 9. Thermoelectric output curve and Seebeck coefficient change of In_2O_3/ITO thermocouple under different atmospheres. (**a**) Thermal voltage output; (**b**) Seebeck coefficient.

Table 3 shows the polynomial fitting results of the curves of the thermocouple under the different heat treatment conditions. The maximum output value of the thermocouple was obtained under the vacuum heat treatment. This was because the thermoelectric output performance of ITO and In_2O_3 varied under the different heat treatment atmosphere conditions. The Seebeck coefficient of ITO and In_2O_3 can be expressed by Equations (3) and (4), respectively [33].

$$S(N_D) = -\left(\frac{\pi}{3N_D}\right)^{2/3} \frac{8\kappa^2 m^* T}{3e\hbar^2}\left(A + \frac{3}{2}\right) \quad (3)$$

$$S(N_D) = -\frac{Ak}{e} - \frac{k}{e}\ln\left(\frac{(2\pi m_e^* KT)^{2/3}}{\hbar^3 N_D}\right) \quad (4)$$

where S is the Seebeck coefficient, N_D is the carrier concentration, κ is the Boltzmann constant, $\hbar$ is the Planck's constant, E is the electronic charge, m^* is the Electronic effective mass, A is the transmission coefficient.

Table 3. Fitting results of output calibration polynomial of In_2O_3/ITO thin film thermocouple.

Type	A (mV/°C^2)	B (mV/°C)	C (mV)	D	R^2	Seebeck Coefficient at 1200 °C Difference (μV/°C)
Vacuum	-1.609×10^{-8}	6.429×10^{-5}	0.084	0	0.9999	138.2
Air	-9.978×10^{-8}	5.557×10^{-5}	0.083	0	0.9999	135.5
N_2	-1.109×10^{-8}	6.542×10^{-5}	0.039	0	0.9999	115.7

The output thermal voltage and the Seebeck coefficient of the overall sensor depend on the changes in the thermoelectric properties of the two electrode materials. After annealing in different heat treatment conditions, the output characteristics of the ITO/In_2O_3 thermocouples have changed. Under the same temperature difference at the cold and hot ends, the sample output value after the heat treatment in the N_2 gas atmosphere was the smallest, caused by N atoms entering the ITO and In_2O_3 thin film structure during high-temperature heat treatment. For ITO, N atoms entering the structure occupied the oxygen

vacancy generated in the sputtering process, which reduced the carrier concentration. The entry of an N atom bonded two free electrons in the film structure, which decreased the concentration of free electrons in the ITO film and increased the Seebeck coefficient of the film electrode. The case of the In_2O_3 thin film was different; it was a non-degenerate semiconductor, and when N atoms entered the film structure, the N atoms acted as a valence band acceptor, which led to the reduction of the output thermoelectric potential of In_2O_3 [32]. Under the influence of these factors, the overall output of the thin film thermocouple treated with the N_2 atmosphere showed a significant downward trend. For the thermocouple samples treated in a vacuum and air at high temperatures, the oxygen vacancy in the thin film electrode decreased after the high temperature in the air atmosphere. Therefore, in the thermoelectric output results, the output value of the sample treated in an air atmosphere was slightly lower than that of the sample treated in a vacuum, which also made the Seebeck coefficient slightly lower when the temperature difference was 1200 °C.

4. Conclusions

ITO/Pt, In_2O_3/Pt and ITO/In_2O_3 thin film thermocouples were prepared on an Al_2O_3 substrate by using the radio frequency magnetron sputtering method. The microstructure of the ITO and In_2O_3 thin films was investigated, and all the ITO and In_2O_3 thin films have a cubic structure, and the annealed film has a relatively dense surface structure. The section structure shows that all the films are continuous without fracture, and the films have a thickness of more than 1.2 μm. At a 900 °C temperature difference, the output of the ITO/Pt and In_2O_3/Pt thermocouples reached 68.7 mV and 183.5 mV, respectively, and the maximum of the Seebeck coefficient was 76.1 μV/°C and 203.9 μV/°C, respectively. The output of the ITO/In_2O_3 thermocouple reached 165.7 mV, and the Seebeck coefficient reached 138.1 μV/°C at a 1200 °C temperature difference. Under thermal shock tests, the ITO/In_2O_3 thermocouples showed good linearity and repeatability from the test results. The high-temperature annealing atmosphere significantly affected the output curve of the thermocouples, so that the output value reached 165.9 mV under a vacuum and 138.9 mV in N_2 conditions, with Seebeck coefficients of 138.2 μV/°C and 115.7 μV/°C, respectively.

Author Contributions: Formal analysis, Y.L., P.S. and W.R.; investigation, Y.L., P.S. and W.R.; writing Y.L., P.S. and R.H.; writing—review and editing, Y.L., P.S. and W.R.; supervision: Y.L., P.S. and R.H. All authors have read and agreed to the published version of the manuscript.

Funding: This research was funded by the Youth Innovation Team Project of Shaanxi Province education department (No. 22JP051).

Data Availability Statement: Not applicable.

Acknowledgments: We appreciate the support from the International Joint Laboratory for Micro/Nano Manufacturing, Measurement Technologies of Xi'an Jiaotong University and Xi'an University of Technology.

Conflicts of Interest: The authors declare no conflict of interest.

References

1. Prashant, A.; Gary, G.W.; Rodrigo, L.A.; Glen, M.; Anthony, B.; Adam, S.; Khellil, S. Leidenfrost heat engine: Sustained rotation of levitating rotors on turbineinspired substrates. *Appl. Energy* **2019**, *240*, 399–408.
2. Christopher, G.; Brooker, R.A.; Marcus, N.; Holger, M. An experimental simulation of volcanic ash deposition in gas turbines and implications for jet engine safety. *Chem. Geol.* **2017**, *461*, 160–170.
3. Tian, B.; Yu, Q.; Zhang, Z.K. Effect of magnetron sputtering parameters on adhesion properties of tungsten-rhenium thin film thermocouples. *Ceram. Int.* **2018**, *44*, S15–S18. [CrossRef]
4. Kenneth, G.K. Thin film transparent thermocouples. *Sens. Actuators A* **1992**, *34*, 95–99.
5. Jih, F.L.; Herbert, A.W. Thin film thermocouples and strain-gauge technologiesfor engine applications. *Sens. Actuators A* **1998**, *65*, 187–193.
6. Usamentiaga, R.; Garcia, D.F.; Molleda, J. Temperature measurement using the wedge method: Comparison and application to emissivity estimation and compensation. *IEEE Trans. Instrum. Meas.* **2011**, *60*, 1768–1778. [CrossRef]

7. Sun, X.G.; Li, Y.H. Review of the development of temperature measurement technology with infrared thermal imager. *Laser Infrared* **2008**, *38*, 101–104.
8. Volinsky, A.A.; Ginzbursky, L. Irradiated Cubic Single Crystal SiC as a High Temperature Sensor. *Mat. Res. Soc. Symp. Proc.* **2004**, 792–798. [CrossRef]
9. Bachuchin, I.V.; Zabusov, O.; Morozov, V.A. Temperature measurement with irradiated materials. *At. Energy* **2011**, *110*, 178–183. [CrossRef]
10. Ruan, Y.F.; Wang, P.F.; Huang, L. High Temperature Sensor Based on Neutron-Irradiated 6H-SiC. *Key Eng. Mater.* **2011**, *495*, 335–338. [CrossRef]
11. Tianshu, L.; Steffen, R. In-situ calibration for temperature-sensitive-paint heat-flux measurement on a finite base. *Int. J. Heat. Mass. Transfer* **2019**, *140*, 420–425.
12. Cheung, W.S. The development of an optical fibre thermometer for gas turbine engines. *Sens. Actuators* **1989**, *19*, 105–117. [CrossRef]
13. Zahra, G.T.; Chen, Y.J.; Liu, Y.Z. End-wall heat transfer of a rectangular bluff body at different heights: Temperature-sensitive paint measurement and computational fluid dynamics. *Appl. Therm. Eng.* **2017**, *122*, 697–705.
14. Tsukamoto, T.; Wang, M.; Tanaka, S. IR sensor array using photo-patternable temperature sensitive paint for thermal imaging. *J. Micromech. Microeng.* **2015**, *25*, 104011. [CrossRef]
15. Ian, M.T.; Otto, J.G. Thin film platinum-palladium thermocouples for gas turbine engine applications. *Thin Solid. Films* **2013**, *539*, 345–349.
16. Kenneth, G.K. Sputtered high temperature thin film thermocouples. *J. Vac. Sci. Technol. A* **1993**, *11*, 1401–1405.
17. Kenneth, G.K. Thin film thermocouples for internal combustion engines. *J. Vac. Sci. Technol. A* **1986**, *4*, 2618–2623.
18. Raoufia, D.; Taherniya, A. The effect of substrate temperature on the microstructural, electrical and optical properties of Sn-doped indium oxide thin films. *Eur. Phys. J. Appl. Phys.* **2015**, *70*, 30302. [CrossRef]
19. Chen, Y.Z.; Jiang, H.C.; Zhao, W.Y. Fabrication and calibration of Pt-10%Rh/Pt thin film thermocouples. *Measurement* **2014**, *48*, 248–251. [CrossRef]
20. Michael, A.M.; James, S.W.; Sanjeev, C. A fast response thermocouple for internal combustion engine surface temperature measurements. *Exp. Therm. Fluid Sci.* **2010**, *34*, 183–189.
21. Tian, B.; Zhang, Z.K.; Shi, P. Tungsten-rhenium thin film thermocouples for SiC-based ceramic matrix composites. *Rev. Sci. Instrum.* **2017**, *88*, 015007. [CrossRef] [PubMed]
22. Anna, N.; James, B.; Jinichiro, N. Failure mechanisms in Pt-Rhx thermocouple sensors caused by gaseous phosphorous species. *Corros. Sci.* **2016**, *103*, 30–41.
23. Kenneth, G.K.; Stephen, S. Thermal and sputtered aluminum oxide coatings for high temperature electrical insulation. *J. Vac. Sci. Technol. A* **1985**, *3*, 2582–2587.
24. Forster, F.; Brack, S.; Poser, R.; Wolfersdorf, J.V.; Weigand, B. A novelsurface-integrated spray-on thermocouple for heat transfer measurements. *Exp. Therm. Fluid. Sci.* **2018**, *93*, 356–365. [CrossRef]
25. Glass, D.E.; Capriotti, D.P.; Reimer, T. Testing of refractory composites for scramjet combusters. *J. Propul. Power* **2016**, *32*, 1550–1556. [CrossRef]
26. Zhao, X.H.; Li, H.T.; Yang, K.; Jiang, S.W.; Jiang, H.C.; Zhang, W.L. Annealing effects in ITO based ceramic thin film thermocouples. *J. Alloys Compd.* **2017**, *698*, 147–151. [CrossRef]
27. Zhang, Z.K.; Tian, B.; Li, L.; Lei, J.M.; Liu, Z.J.; Liu, J.J.; Cheng, G.; Zhao, N.; Fang, X.D.; Zhao, L.B. Thermoelectricity and antivibration properties of screen-printed nanodoped $In_{1.35}ZnO_{2.11}/In_2O_3$ thin film thermocouples on alumina substrates. *Ceram. Int.* **2022**, *48*, 25747–25755. [CrossRef]
28. Chen, X.; Otto, J.G.; Matin, A. Thin film Thermocouples Based on the System In_2O_3–SnO_2. *J. Am. Ceram. Soc.* **2011**, *94*, 854–860. [CrossRef]
29. Ian, M.T.; Matin, A.; Otto, J.G. Metallic and Ceramic Thin Film Thermocouples for GasTurbine Engines. *Sensors* **2013**, *13*, 15324–15347.
30. John, D.W.; Gustave, C.F.; Zhu, D.M. Ceramic thin flm thermocouples for SiC-based ceramic matrix composites. *Thin Solid. Films* **2012**, *520*, 5801–5806.
31. Otto, J.G.; Matin, A.; Ian, M.T. Stability and Microstructure of Indium Tin Oxynitride Thin Films. *J. Am. Ceram. Soc.* **2012**, *95*, 705–710.
32. Otto, J.G.; Eike, B.; Gustave, C.F. Preparation and characterization of ceramic thin film thermocouples. *Thin Solid Films* **2010**, *518*, 6093–6098.
33. Gregory, O.J.; You, T.; Crisman, E.E. Effect of aluminum doping on the high-temperature stability and piezoresistive response of indium tin oxide strain sensors. *Thin Solid Films* **2005**, *476*, 344–351. [CrossRef]